UC Irvine
UC Irvine Previously Published Works

Title

Effect of Surface Heterogeneity on the Boundary-Layer Height: A Case Study at a Semi-Arid Forest

Permalink

https://escholarship.org/uc/item/6z33w0nw

Journal

Boundary-Layer Meteorology, 169(2)

ISSN

0006-8314

Authors

Brugger, Peter
Banerjee, Tirtha
De Roo, Frederik
et al.

Publication Date

2018-11-01

DOI

10.1007/s10546-018-0371-5

Peer reviewed

RESEARCH ARTICLE

CrossMark

Effect of Surface Heterogeneity on the Boundary-Layer Height: A Case Study at a Semi-Arid Forest

Peter Brugger[1] · **Tirtha Banerjee[1,2]** · **Frederik De Roo[1]** · **Konstantin Kröniger[1]** · **Rafat Qubaja[3]** · **Shani Rohatyn[3]** · **Eyal Rotenberg[3]** · **Feodor Tatarinov[3]** · **Dan Yakir[3]** · **Fulin Yang[3]** · **Matthias Mauder[1]**

Abstract

We investigate the effects of an isolated meso-γ-scale surface heterogeneity for roughness and albedo on the atmospheric boundary-layer (ABL) height, with a case study at a semi-arid forest surrounded by sparse shrubland (forest area: 28 km^2, forest length in the main wind direction: 7 km). Doppler lidar and ceilometer measurements at this semi-arid forest show an increase in the ABL height over the forest compared with the shrubland on four out of eight days. The differences in the ABL height between shrubland and forest are explained for all days with a model that assumes a linear growth of the internal boundary layer of the forest through the convective ABL upwind of the forest followed by a square-root growth into the stable free atmosphere. For the environmental conditions that existed during our measurements, the increase in ABL height due to large sensible heat fluxes from the forest (600 W m^{-2} in summer) is subdued by stable stratification in the free atmosphere above the ABL, or reduced by high wind speeds in the mixed layer.

1 Introduction

As the lowest part of the atmosphere, the atmospheric boundary layer (ABL) is directly influenced by the underlying surface (Stull 1988), and controls the exchanges of heat, momentum and pollutants between the free atmosphere and Earth's surface. Concepts relating to the ABL, such as scaling laws, usually assume a horizontally homogeneous surface (Lenschow

---

✉ Peter Brugger
   peter.brugger@kit.edu

[1]   Institute of Meteorology and Climate Research, Atmospheric Environmental Research, Karlsruhe Institute of Technology, Kreuzeckbahnstraße 19, 82467 Garmisch-Partenkirchen, Germany

[2]   Present Address: Earth and Environmental Sciences Division, Los Alamos National Laboratory, Los Alamos, NM 87545, USA

[3]   Department of Earth and Planetary Sciences, Faculty of Chemistry, Weizmann Institute of Science, 234 Herzl Street, 7610001 Rehovot, Israel

et al. 1980; Sun et al. 2013). However, the Earth's surface is mostly inhomogeneous due to variations in topography and land cover, which has implications for a range of atmospheric transport processes (Rotach et al. 2014). The effects of heterogeneity on the ABL depend on the horizontal scale and amplitude of the surface heterogeneities (Mahrt 2000). The horizontal scales of atmospheric processes are often grouped by their size into three classes: macroscale, mesoscale and microscale, with further subdivision of each class into α, β and γ scales (Orlanski 1975). The importance of macroscale surface heterogeneity (e.g. the land–sea distribution and mountain ranges) in numerical weather prediction is known and recognized, but the importance of the smaller mesoscale (e.g. forests, lakes and cities) and microscale (e.g. forest edges, buildings) surface heterogeneities for the ABL is still uncertain (Maronga and Raasch 2013).

Mesoscale surface heterogeneity studies have shown a range of effects. For example, analytical investigations of thermal heterogeneities by Dalu et al. (1996) showed that these can enhance vertical heat fluxes and that the synoptic background flow weakens the effects. Mauder et al. (2007) found from airborne flux measurements over lakes that the meso-γ-scale contributions to turbulent fluxes may be related to the energy-balance residual, which is a systematic difference between the available energy and turbulent energy observed at micrometeorological sites. Studies of flows over forest edges and clearings show enhanced turbulence levels, modified integral length scales and increased spectral slopes for the velocity fluctuations (Träumner et al. 2012; Eder et al. 2013; Kanani et al. 2014). Studies using large-eddy simulation have investigated the effect of surface heterogeneity on the entrainment flux (Sühring et al. 2014), dispersion (Gopalakrishnan and Avissar 2000; Wu et al. 2009), horizontal wind speed (Kang et al. 2012) and the development of secondary circulations (Maronga and Raasch 2013) and coherent structures (Baidya Roy and Avissar 2000).

The ABL height describes the vertical extent of the region in which the atmosphere is directly influenced by the Earth's surface, and is used in surface-layer parametrizations as an outer-layer scaling parameter (Banerjee and Katul 2013) for the influence of the exchange between the land surface and the atmosphere (Zilitinkevich et al. 2012). The ABL height is highly variable in time and space depending on topography, the underlying surface, synoptic conditions, and the time of day. Encroachment models neglecting dynamic effects and only accounting for thermodynamical influences predict a deeper ABL for stronger surface heating and for a given mixed-layer temperature (Batchvarova and Gryning 1991). Surface roughness in the presence of a background flow increases the turbulence levels and deepens the ABL as well, but heating and cooling effects are more important for convective conditions (Stull 1988). While studies on the influence of surface heterogeneity on the ABL height are scarce, Zhong and Doran (1995) found from numerical simulations of farm and steppe surfaces that the height of the convective ABL is controlled by the local surface heat flux and roughness, together with horizontal advection and vertical motions arising from convergence or divergence. Using ground-based remote-sensing instruments, De Tomasi et al. (2011) observed a decrease in the ABL height due to a replacement of continental air with maritime air related to the onset of a sea breeze at a coastal site. Huang et al. (2017) investigated the diurnal cycle of the ABL height over a city, and reported a deeper nocturnal boundary layer, which they explained as being due to heat absorbed during the day by man-made structures followed by the night-time release in the form of thermal updrafts.

We investigate the effect of meso-γ-scale surface heterogeneities on the ABL height by focusing on the Yatir forest in Israel, which is an isolated, semi-arid forest surrounded by shrubland (Fig. 1), with pronounced differences in albedo and roughness compared with the surrounding shrubland, making it useful for the study of the effects of surface heterogeneity. Rotenberg and Yakir (2011) analyzed the impact of the Yatir forest on the surface-energy

budget, showing an increased surface radiation budget and higher sensible heat fluxes compared with the shrubland. Using the blending-height concept, Eder et al. (2015) estimated that the areal extent of the Yatir forest is of a sufficient magnitude to be able to influence the whole depth of the ABL, and found evidence for the existence of a secondary circulation between the forest and surrounding shrubland.

Our aim here is to investigate whether albedo and roughness heterogeneities with horizontal extent within the meso-γ-scale can modify the whole depth of the ABL. To achieve this aim, we use a case study at the Yatir forest, and (i) investigate the forest's effect on the ABL height, and (ii) develop a model describing the effects.

2 Measurements

We describe our study site at the Yatir forest and the measurement set-up here, followed by the instruments used and the data-processing procedures followed for eddy-covariance stations, Doppler lidars, as well as for the ceilometer and radiosondes.

2.1 Research Site

The evergreen Yatir pine forest, which is located in southern Israel to the west of the Dead Sea and north of the Negev desert (Fig. 1), is a planted forest covering an area of approximately 28 km^2, with a length of 7 km in the main wind direction, and *Pinus halepensis* as the predominant tree species (Rotenberg and Yakir 2011). The climate is semi-arid with an annual mean precipitation of 285 mm and an annual net positive surface radiation budget of 238 W m^{-2} (Rotenberg and Yakir 2011). The Yatir forest has a mean height of 662 m above sea level, with its lowest areas at 500 m and highest at 850 m. The older north-western parts of the forest with tree heights of around 11 m were planted from 1964–1969, and planting has continued since. The forest represents isolated heterogeneity for albedo, roughness and surface (skin) temperature compared with the surrounding shrubland. The albedo of the forest is 0.13 compared with 0.34 for the shrubland, and the skin temperature of the forest is 5°C lower on average (Rotenberg and Yakir 2011). The shrubland consists of scattered herbaceous annuals and perennials (mainly *Sarcopoterium spinosum*) with heights ranging from 0.3–0.5 m. During the summer dry season, this leads to sensible heat fluxes of up to 600 W m^{-2} during midday, and friction velocities of 0.8 m s^{-1} over the forest canopy, which are twice as high as those of the surrounding shrubland (Eder et al. 2015).

2.2 Measurement Set-Up and Synoptic Conditions

To observe the effects of the forest on the ABL, three measurement sites were established along the main wind direction (Fig. 1):

1. Upwind of the forest (latitude 31.3757°, longitude 35.0242°, 620 m above sea level) to probe the ABL with a Doppler lidar and eddy-covariance station without disturbance from the forest.
2. In the forest (latitude 31.3453°, longitude 35.0522°, 660 m above sea level) to investigate the effect of the forest on the ABL with a Doppler lidar and eddy-covariance station.
3. Downwind of the forest (latitude 31.3258°, longitude 35.0838°, 780 m above sea level) to capture the advection of these effects with a ceilometer.
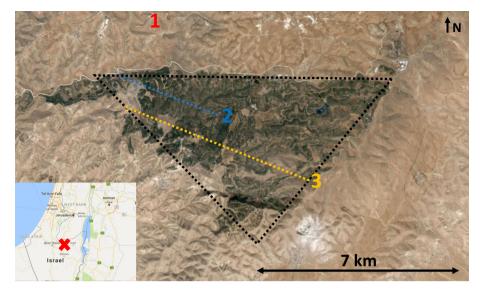
Fig. 1 Satellite image of the Yatir forest with the three measurement sites shown as coloured numbers (see Sect. 2.2). Map of Israel with the location of forest (bottom left, location marked with red cross; the distance from the Mediterranean Sea is approximately 60 km). The dashed lines show the geometry of the heterogeneous model introduced in Sect. 3.2 with the black line showing the approximated shape of the forest and the blue (orange) line showing the distance Δd to the forest edge in the main wind direction for the forest site (downwind site) for 29 August 2015 with a wind direction of 292° as an example. Source of map and satellite image: Google Maps

The measurements were conducted from 16–29 August 2015 during the dry season when the albedo difference between the desert and forest is more pronounced compared with the wet season. During the time of the measurements, the area was located within the subtropical ridge, which is an area of general subsidence in the troposphere connected to the sinking branch of the Hadley cell (Barry and Chorley 2003). The synoptic horizontal pressure gradients are controlled by a heat-induced surface low to the east, the Persian trough (Dayan and Rodnizki 1999), giving a main wind direction from the north-west and cloud-free conditions, with a radiation-driven diurnal cycle of the ABL during the campaign.

2.3 Eddy-Covariance Method

We measured the turbulent fluxes at the upwind and forest sites with two eddy-covariance stations. Measurements at the upwind site consisted of a mobile eddy-covariance station from the Weizmann Institute of Science, with an expandable mast equipped with an R3-100 ultrasonic anemometer (Gill Instruments, Lymington, Hampshire, UK) and a LI-7200 gas analyzer (LI-COR Biosciences, Lincoln, Nebraska, USA). The sampling frequency was 20 Hz, and the measurement height was 9 m above the ground until 23 August 2015, before being raised to 15 m to blend local terrain irregularities because of problems with the stationarity assumption due to a small footprint. Both measurement heights are within the surface layer, where fluxes are assumed in theory to be constant with height, which is also approximately the case in these measurements (Aubinet et al. 2012).

The eddy-covariance station at the forest site is the permanent FLUXNET Yatir forest station (Baldocchi et al. 2001), which is equipped with an R3-50 ultrasonic anemometer

from Gill Instruments and a LI-7000 gas analyzer from LI-COR Biosciences, with both instruments sampling at a frequency of 20 Hz. The ultrasonic anemometer is mounted 19 m above the ground on a tower surround by trees of an average height of 10 m, placing the ultrasonic anemometer 9 m above the roughness elements. The eddy-covariance data at the forest are missing on 20 August 2015 from 0308–1750 UTC and on 25 August 2015 from 0910–1500 UTC due to data-acquisition problems.

Computation of the turbulence statistics at 30-min intervals, and the quality control of the eddy-covariance data from both stations, were performed with the TK3 software (Mauder and Foken 2015), which includes despiking (Mauder et al. 2013), unit conversions (Schotanus et al. 1983), a transformation of the coordinate system according to the planar-fit method (Wilczak et al. 2001), block averaging, and the determination of time lags by cross-correlation and frequency-response corrections (Moore 1986). The quality control includes steady-state and integral-turbulence tests (Foken and Wichura 1996), with low-quality data discarded based on the flagging system of Mauder et al. (2013).

2.4 Doppler Lidar

Together with the eddy-covariance stations, two Doppler lidars (the Stream Line model, Halo Photonics Ltd., Worcester, UK) were deployed at the upwind and forest sites, and levelled using the internal pitch and roll sensors (instrument specifications in Table 1). Both systems were operated in vertical stare mode with an 18-point velocity-azimuth-display scan at an elevation angle of 70° every 30 min, and every full hour the instrument performed some housekeeping for 30 sec. Wind-speed and direction profiles were computed from the velocity-azimuth-display scans with the method described in Browning and Wexler (1968). Data quality was ensured by averaging 15,000 pulses per estimate for an effective measurement frequency of 1 Hz, while discarding range gates from the lowest 60 m or with a signal-to-noise ratio < −17 dB (Päschke et al. 2015). The Doppler lidar at the upwind site was inoperable due to power cuts from 1500 UTC on 19 August 2015 until 1030 UTC on 21 August 2015, and for a short time on 23 August 2015 around 1000 UTC.

Several methods exist for the determination of the ABL height from ground-based lidars (Lammert and Bösenberg 2006; Hennemuth and Lammert 2006; Träumner et al. 2011), for which we used the gradient method outlined in Münkel et al. (2007), which detects the ABL height by a decrease in the backscatter coefficient between the aerosol-laden ABL and the clean, free atmosphere. The backscatter coefficient profiles were first range corrected, vertically smoothed, while removing noise at large distances. The heights of the largest of three negative gradients above a threshold were then computed for each backscatter profile, and the most frequent heights within each 10-min interval were detected as aerosol-layer heights. To compute the time series of the ABL height from the aerosol layers, and to remove outliers, we followed the algorithm of Lotteraner and Piringer (2016), but without their wind-speed threshold. First, we selected the lowest detected aerosol layer for each timestep, and then outliers were filtered by removing values lower than 100 m, higher than 2500 m, or differing by more than 200 m from the moving average of 1 h.

2.5 Ceilometer

A ceilometer model CL51 from Vaisala (Vantaa, Finnland) was deployed at the downwind edge of the forest pointing vertically upwards to measure profiles of the backscatter coeffi-

Table 1 Technical specification of the two Halo-Photonics Stream Line Doppler lidars used at the upwind site and the forest site (left column) and the Vaisala C51 ceilometer (right column) at the downwind site

Serial number (upwind/forest)	0114-75/0114-74	F4460004
Range gate length (m)	18	10
Pulse length (m)	60	33
Pulse repetition frequency (Hz)	15,000	6500
Laser wavelength (μm)	1.5	0.91

cient. The ceilometer was levelled with a spirit level, and sampled at a temporal resolution of 16 s; the technical specifications are given in Table 1.

Data processing and detection of the largest negative gradients in the backscatter coefficient profiles were performed with the BLMatlab software version 1.9 (Münkel et al. 2007). The algorithm of Lotteraner and Piringer (2016) was also used to compute the time series of the ABL height from Doppler lidar data. Estimates of the ABL height can differ depending on the definition, instrument or algorithm used (Seibert et al. 2000). Side-by-side measurements of the ABL height showed good agreement for convective, cloud-free conditions between the Doppler lidar and ceilometer (see "Appendix 1").

2.6 Radiosonde

Information on the stratification of the free atmosphere was obtained from temperature profiles derived from radiosondes launched at Beit Dagan (station number 40179, which is located approximately 75 km from the Yatir forest), which uses RS92/DigiCORA II radiosondes from Vaisala (Vantaa, Finnland). Based on the results of a World Meteorological Organization inter-comparison of radiosondes in Yangjiang, China, the radiosonde has an accuracy of 0.5 K for the temperature, 1 hPa for the pressure, and 20 m for the height in the lower atmosphere. A radiosonde ascending at 5 m s^{-1} corresponds to a 50-m layer averaged over 10 s (Dayan et al. 2002). The Israel Meteorological Service conducted the launches, whose resulting data were distributed via the World Meteorological Organization network, which we accessed at a web portal provided by the University of Wyoming (www. weather.uwyo.edu).

To determine the stratification of the free atmosphere, we first determined the ABL height from the radiosonde profiles using the parcel method as reviewed by Seibert et al. (2000), but without adding an excess temperature. With this method, the ABL height is determined from a temperature inversion at the top of the mixed layer by following the dry adiabat from the lowest sounding level until it intersects with the temperature profile. The results were found to be in agreement with a subjective method by visually locating an inversion base with a simultaneous dew-point decrease. The 1200 UTC soundings coincide with the local temperature maximum when the ABL has already incorporated the residual layer. The stratification of the free atmosphere was then computed from the potential-temperature gradient γ_L of a 500-m layer starting at the detected ABL height. An alternative approach of computing γ_L from a fixed height interval above the ABL (1500–2000 m) leads to similar results, with the exception on 29 August 2015 when a second elevated inversion was present, so that the parcel method is preferable (not shown). The measurement accuracy leads to an upper error bound of 0.002 K m^{-1} for the potential-temperature gradient. We can assume that the temperature gradient at Beit Dagan is representative for the Yatir forest, because

the horizontal variation of the free atmosphere in the subtropical ridge is small (Barry and Chorley 2003).

3 Models of the Boundary-Layer Height

To identify mechanisms affecting the ABL height, we considered two models that take into account the flux at the surface and the stratification of the free atmosphere, with the first assuming horizontal homogeneity, and the second accounting for a change in surface properties.

3.1 Homogeneous Model

The ABL height z_i was computed using a thermodynamic encroachment model, with entrainment at the boundary-layer top given by

$$\frac{dz_i}{dt} = \frac{\overline{w'\theta'} - \overline{w'\theta'}_{z_i}}{\gamma_L z_i},$$ (1)

where $\overline{w'\theta'}$ is the kinematic heat flux at the surface, $\overline{w'\theta'}_{z_i}$ is the entrainment flux at the boundary-layer top, and γ_L is the potential-temperature gradient of the free atmosphere above the ABL (Carson 1973; Zilitinkevich et al. 2012). For encroachment models, the entrainment flux is usually assumed to be proportional to the sensible heat flux at the surface by $\overline{w'\theta'}_{z_i} = -\beta \overline{w'\theta'}$ (Tennekes 1973), where the value of β (= 0.2) is frequently assumed constant (Betts and Ridgway 1989; Juang et al. 2007). The model assumes both horizontal homogeneity and the boundary layer as a single slab without any internal source or sink terms (Juang et al. 2007). The ABL height was computed by integrating Eq. 1 from 0600–1300 UTC. As an initial condition, the ABL height measured by the Doppler lidars at 0600 UTC is used, which is the earliest time when reliable measurements of the ABL height are available at all sites and for all days. We used $\overline{w'\theta'}$ derived from the eddy-covariance measurements at the respective sites for each timestep, and set the value of γ_L as constant for the whole day based on the 1200 UTC radiosonde profile at Beit Dagan. For comparison with measurements, the computed ABL heights were averaged from 1000–1300 UTC.

3.2 Heterogeneous Model

The heterogeneous model for describing the ABL height over the forest accounts for the both heterogeneity and the presence of a convective boundary layer upwind of the forest, where a schematic overview of the growth process is shown in Fig. 2. We assume an air parcel travels close to the surface from the shrubland to the forest at a mean horizontal wind speed u_m, and rises convectively at the convective velocity scale $w_* = (g z_i \overline{w'\theta'} \theta^{-1})^{1/3}$ (Deardorff 1970), continuing to rise until reaching the top of the ABL, whose height is not yet influenced by the forest. The distance the air parcel travels horizontally until it reaches the ABL height is given by

$$\Delta x_1 = u_m \frac{z_i}{w_*},$$ (2)

where u_m is the mixed-layer wind speed computed from the Doppler-lidar measurements and averaged between 250 and 1000 m above the ground, z_i is the ABL height from the
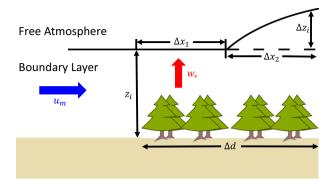
Fig. 2 Schematic image of the increase in the ABL height over the forest as explained in Sect. 3.2

upwind site measured by the Doppler lidar, and w_* is computed with values from the eddy-covariance station at the forest site. Once at the top of the ABL, an air parcel penetrates the free atmosphere, which deepens the ABL over the forest, similar to the offshore growth of a convective internal boundary layer encountering a stably-stratified atmosphere, assuming air parcels travel along straight trajectories. To compute the increase in the ABL height, we adapted the model of Venkatram (1977) given by

$$\Delta z_i = \frac{u_*}{u_m} \left(\frac{2(\theta_f - \theta_d)\Delta x_2}{\gamma_L(\beta^2(2\beta + 1))^{-1}} \right)^{1/2},$$ (3)

where u_* is the friction velocity of the forest, $\Delta x_2 = \Delta d - \Delta x_1$ is the distance the air parcel travels while working against the free atmosphere after reaching the top of the upwind ABL, Δd is the distance to the forest edge in the wind direction (Fig. 1), and θ_f and θ_d are the potential air temperatures over the forest canopy and at the desert, which are assumed to be constant for both surface types. This assumption can be made because both the shrubland and the forest are horizontally homogeneous within their domain, and, close to the surface, the effects of advection should only matter close to the forest edge (Dupont and Brunet 2008; Kröniger et al. 2017). Furthermore, the model also assumes steady-state conditions for the time scale of the model (≈ 3 h), which may be unsatisfactory during the hours around sunset and sunrise (Venkatram 1977). The distance Δd was computed by approximating the forest shape with a triangle as shown in Fig. 1. The increase in the ABL height was computed for each day based on mean values from 1000–1300 UTC around the time of maximum ABL height, which implicitly assumes that these conditions are stationary for a sufficient time such that the effects are transported to the top of the ABL.

4 Results

We first investigate whether the Yatir forest acts to increase the ABL height z_i compared with that over the upwind site. If the forest has an effect on the magnitude of z_i, it is expected that the largest differences between sites occur at the time of the maximum value of z_i, corresponding to between 1000 UTC and 1250 UTC at each site (Table 2). The mean z_i value from 1000–1300 UTC for each day at each site is shown in Fig. 3a (the period is extended to 1300 UTC for consistency with the 30-min eddy-covariance data presented below). Features of note are a general increase in the value of z_i from 22–28 August 2015 at

Table 2 Time of maximum ABL height according to Doppler lidar and ceilometer data for each site and day

Date	Upwind	Forest	Downwind
22 August 2015	1200	1140	1200
23 August 2015	1210	1140	1200
24 August 2015	1120	1140	1200
25 August 2015	1050	1250	1140
26 August 2015	1150	1150	1240
27 August 2015	1100	1100	1110
28 August 2015	1040	1030	1200
29 August 2015	1000	1020	1040

all three sites, a period from 22–25 August 2015 when the value of z_i is similar at the three sites, and a period from 26–29 August 2015 with an increase in z_i values from the upwind to downwind of the forest. The mean difference between the upwind and downwind sites during the period with similar z_i values at all sites is 19 m, but 122 m during the period with an increase in z_i values over the forest. The root-mean-square error between the instruments is 48 m (see Appendix 1 for side-by-side comparisons of the Doppler lidar and ceilometer measurements). By investigating the periods around the time of maximum ABL height, we also avoid detection problems associated with multiple layers of weak aerosol-density changes during the night, and periods without a fully convective boundary layer.

The potential-temperature gradient of the free atmosphere above the ABL is shown in Fig. 3b, illustrating larger values during more stable stratification from 22–25 August 2015 compared with smaller values from 26–29 August 2015 corresponding to less stable stratification. The accuracy of the potential-temperature gradient is 0.002 K m^{-1}, which is sufficient to separate the two periods. The period with more stable stratification coincides with similar z_i values at all three sites, while the period with a less stable stratification coincides with an increase in z_i values over the forest. The change in stratification may explain the site differences, because the ABL requires energy to penetrate the free atmosphere against stable stratification, and the required energy increases with stability. Moreover, the energy input for the ABL growth from the sensible heat fluxes did not vary much from day to day during the campaign (the mean values from 1000–1300 UTC varied to within 16% of the campaign mean as shown in Fig. 6b). The change in the potential-temperature gradient is presumably caused by the southern extension of a Rossby-wave passage in the westerlies, which changed the curvature of the isohypses from anticyclonic to cyclonic, and cooled the free atmosphere (Global Forecast System reanalysis). Both indicate that the large-scale subsidence was reduced in the eastern Mediterranean, which weakened the stable stratification in the lower free atmosphere.

The effect of stratification on the general increase in z_i values at all three sites from 22–28 August 2015 is investigated using the homogeneous-slab model (Eq. 1) without consideration of the free-atmosphere stratification, which predicts constant z_i values throughout the campaign, and overestimates z_i over the forest on all days compared with the measurements (Fig. 4a). The model including the stratification from the radiosonde data predicts a value of z_i roughly similar to the measurements for the upwind site with the exception of measurements on 25 August 2015 (the absolute mean difference excluding 25 August 2015 is 109 m), but always shows an overestimated value of z_i at the forest (Fig. 4b). Since the background flow speed was higher on 25 August 2015 than on any other day during the campaign (see Fig. 6a), the failure of the model on this day may be explained by the model only accounting
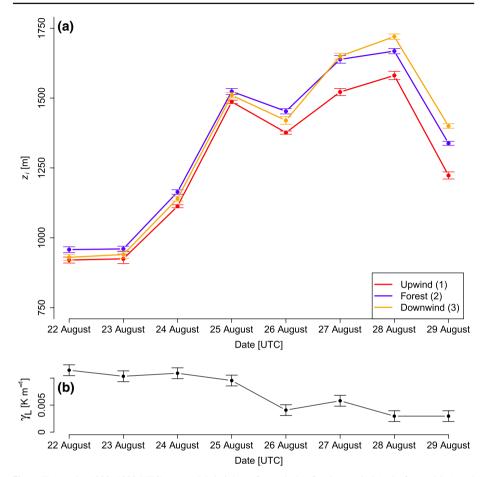
Fig. 3 Top **a**: the 1000–1300 UTC mean ABL height z_i for each day for the upwind (red), forest (blue) and downwind (orange) sites as detected by a drop in the aerosol density from the backscatter profiles of the lidars using the methods described in Sects. 2.4 and 2.5. The error bars show the standard error of the mean. Bottom **b**: time series of the 1200 UTC values of the potential-temperature gradient γ_L of the free atmosphere above the ABL computed from radio soundings at Beit Dagan as described in Sect. 2.6. The error bars show the error bounds of γ_L values based on the accuracy of the radiosonde measurements

for buoyancy-driven growth of the boundary layer. A second exception is 29 August 2015, which has lower z_i values despite a low potential-temperature gradient (Fig. 3b), but this decline is reproduced by the model for the upwind site. This result suggests that the general increase in z_i values at all three sites is connected to a decrease of the stable stratification of the free atmosphere above the ABL from 0.010 to 0.004 K m^{-1}, but cannot explain all the variation of z_i alone. However, these results show that the boundary layer over the forest site is not yet fully adapted to the new surface.

The increase in ABL height from the upwind site to the forest or downwind site Δz_i is investigated with the heterogeneous model (Eq. 3). Figure 5a shows a comparison of the predicted and measured Δz_i values by the model and Doppler lidars, respectively, for the forest site, which agree within the margin of the standard error of the measurements. For the conditions prevailing during the campaign, the value of Δz_i is mainly controlled by the
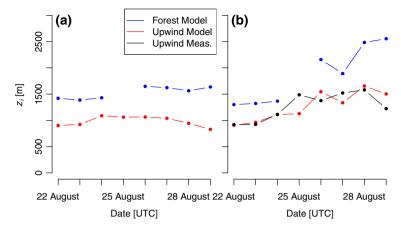
Fig. 4 Mean values of z_i from 1000–1300 UTC for each day for the upwind (red) and forest (blue) sites computed with the homogeneous model (Eq. 1). The left panel **a** shows the predicted z_i values based on the measured sensible heat flux at the eddy-covariance stations and a constant potential-temperature gradient of $\gamma_L = 0.01$ K m^{-1}. The right panel **b** shows the results using the value of γ_L obtained from the radiosonde launches at Beit Dagan shown in Fig. 3b. For comparison, the measured z_i values for the upwind site as shown in Fig. 3a are plotted in the right panel (black)

combination of the stratification of the free atmosphere (see Fig. 3b) and the background flow in the mixed layer (see Fig. 6a), which enters Eq. 3 twice by also influencing the magnitude of Δx_2. The variations of the sensible heat flux, the friction velocity, and temperature differences (see Fig. 6b–d) do not have a strong impact on the results, either because their variations during the campaign were too small, or because the magnitude of Δz_i is not sensitive to any variations. The results for the downwind site have large deviations from the measurements during the first period with a more stable stratification in the free atmosphere, but show agreement with the measurements for the period with less stable stratification (Fig. 5b). Theories concerning the structure of the convective ABL over complex terrain suggest that a strong capping inversion makes the ABL height less terrain-following (De Wekker and Kossmann 2015; Stull 1992), which may explain the overestimation for the downwind site during the first period, because the site is located on a ridge at a higher elevation than the other two sites, and the heterogeneous model assumes a terrain-following ABL.

In summary, the results of this campaign suggest that, while the ABL is not in complete equilibrium with the forest, its effects have propagated through the whole depth of the ABL, which increases the ABL height if the stratification in the free atmosphere above the ABL is weak. However, high wind speeds increased the distance air parcels travel before reaching the ABL top, and reduced the forest's effect on the ABL height.

5 Discussion

The dependency of the general ABL height in Israel on the upper-air inversion by the subtropical anticyclone (Dayan and Rodnizki 1999), as well as the dependency on the sensible heat flux and friction velocity of the underlying surface for homogeneous conditions, have been established (e.g. Batchvarova and Gryning 1991; Zilitinkevich et al. 2012). Studies of the ABL height in the presence of surface heterogeneity at shorelines with a stable boundary layer offshore have detected a developing convective internal boundary layer being stabilized
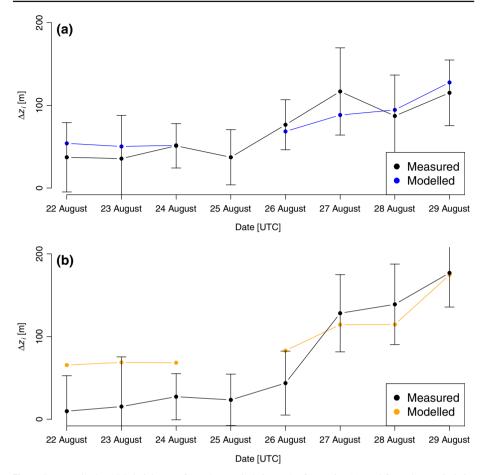
Fig. 5 Increase in the ABL height Δz_i from the upwind site to the forest site (**a**), and from the upwind site to the downwind site (**b**) according to lidar measurements (black) averaged from 1000–1300 UTC. The error bars show the sum of the standard error of both instruments. The predicted increase by the heterogeneous model given by Eq. 3 is shown for the forest (blue) and the downwind site (orange). The model was computed with the mean values calculated from 1000–1300 UTC shown in Fig. 6a–f and the value of γ_L from 1200 UTC shown in Fig. 3b

in the upper layer by the stable stratification (Garratt 1990; De Tomasi et al. 2011). Similar processes are also applicable at our study site, but are elevated to the ABL top and shifted horizontally downwind, because a well-mixed convective ABL from the desert is advected over the forest where the internal boundary layer deepens rapidly initially. After the forest's effects reach the top of the upwind ABL, the growth of the ABL slows as it penetrates deeper into the free atmosphere. The main driver for the increase in the magnitude of z_i over the forest is the large sensible heat flux from the forest during the day, which often exceeds 600 W m^{-2}, which is twice as high as that of the surrounding shrubland, and results from the lower albedo of the forest compared with the surrounding shrubland (Rotenberg and Yakir 2010). Furthermore, the enhanced roughness of the canopy enhances the magnitude of the heat flux at a lower surface temperature than would be required for a smoother surface (Banerjee et al. 2017). While the large sensible heat fluxes of the forest were present on all
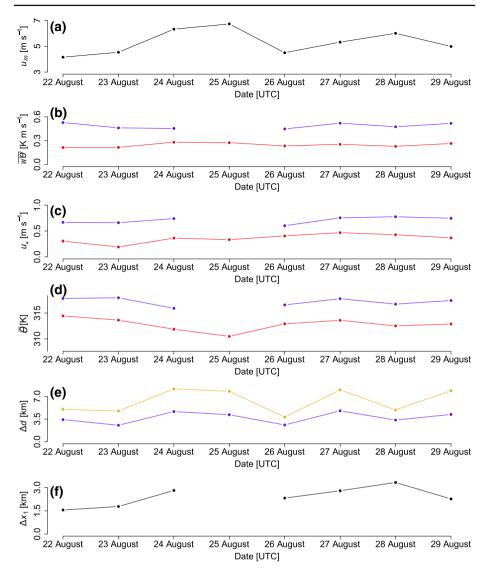
Fig. 6 Time series of the mean values from 1000–1300 UTC of the horizontal wind speed averaged between 250 m and 1000 m above ground level from the Doppler lidars (**a**), the kinematic sensible heat flux (**b**), the friction velocity (**c**), and the potential temperature for 1000 hPa (**d**) over the forest canopy (blue) and the desert surface (red) derived from the eddy-covariance stations. Panel **e** shows the distance Δd in the wind direction from the forest site (blue) and downwind site (orange) to the forest edge for the geometry explained in Sect. 3.2 and shown in Fig. 1. Panel **f** shows the distance Δx_1 (Eq. 2) air parcels travel before reaching the top of the upwind ABL

days of the campaign, their effect on the value of z_i was suppressed by a more stable stratification in the free atmosphere on some days. High wind speeds also opposed the increase in z_i values by increasing the required distance of the first growth phase through the advected upwind ABL, so that the size of the forest became too small to have any significant effect. As the two opposing mechanisms affecting the ABL height were independent, the change of the inversion at the boundary-layer top cannot be linked to surface data.

As our results may be influenced by topographical effects and a bias in the detection of the ABL height by the ceilometer and Doppler lidar instruments, both effects are discussed below. The convective boundary layer over complex terrain is expected to be shallower over mountains and deeper over valleys from noon to the evening (De Wekker and Kossmann 2015). The topography of the Yatir forest has a higher elevation at the downwind site compared with the upwind site. As the effects of advection due to the north-western background flow would reduce the magnitude of z_i for the forest and downwind site (De Wekker and Kossmann 2015), the influence of the topography opposes the increase in the magnitude of z_i by the forest, and the height difference between the measurement sites would cause an underestimation of Δz_i values in the measurements for our assumption of a terrain-following ABL.

As we used a different instrument at the downwind site to detect the ABL height than at the forest and upwind sites, a bias between the instruments may distort the results. A comparison of the site-by-site measurements based on Doppler lidar and ceilometer data is presented in Appendix 1, showing that the bias between the instruments is smaller than the increase in the magnitude of z_i due to the effect of the forest. Here, we assume that the bias between the two identical Doppler lidars is smaller than the bias between the Doppler lidar and the ceilometer.

Further limitations of the results arise from the lack of validation data for those periods except at the time of the maximum ABL height, as well as the inability of the heterogeneous model to reproduce fluctuations in Δz_i values on short time scales. The former limitation was partly a precision problem, because the measured Δz_i values before the time of the maximum ABL height were not significant, and later in the afternoon when residual layers were encountered. Also, the model assumption of a steady state may be violated due to the diurnal cycle of z_i values for those times. The latter limitation results from fluctuations in ABL height due to entrainment, as well as the penetration of thermals into the free atmosphere on short time scales (tens of minutes). This process is not included in the model and, if it were to be included, our measurement set-up would be insufficient for verification because we cannot track individual thermals. Furthermore, the presence of topography with a non-terrain-following ABL impedes correct model estimates.

The results presented herein have shown that the Yatir forest may influence the entire ABL, which does not fully adapt to the forest whose area is limited. As the planting of the Yatir forest (and other forests in the area) continues, a larger forest will presumably have a stronger impact on the ABL height. Based on the magnitude of the forest's sensible heat flux, an increase in the boundary-layer height by roughly 500 m is predicted by the homogeneous model (Fig. 4). Using the heterogeneous model, we increased the forest size Δd until it yielded the expected 500-m increase of the homogeneous case, which requires a forest on the scale of 72 km, or approximately ten times the size of the current forest.

6 Conclusion

Measurements of the ABL height z_i show that a semi-arid forest with a horizontal extent within the meso-γ scale surrounded by shrubland can lead to increases in the magnitude of z_i, with the effect advected downwind. The increase in z_i values over the forest is driven by the large sensible heat flux generated in this dry ecosystem, but is constrained by the stratification of the free atmosphere above the ABL top, as well as the wind speed in the mixed layer. Days with a potential-temperature gradient of $\gamma_L > 9 \times 10^{-3}$ K m^{-1} prevented

a significant increase in z_i values over the forest, while an increase of $70-260$ m was observed for days with $\gamma_L < 5 \times 10^{-3}$ K m^{-1}. High wind speeds reduced the increase in the magnitude of z_i due to the shorter adjustment period of the boundary layer to the forest. However, the increase is still detectable for wind speeds up to 6 m s^{-1} during our measurement period. As these findings are based on only eight days of measurements, an extended campaign to yield more robust results over a wider range of meteorological conditions is desirable for future research.

The measured increase in z_i values resulting from the presence of the forest is able to be reproduced with a modified internal boundary-layer model (Eq. 3), which is a new model assuming a vertical transport of the forest's effects at the convective velocity scale w_* to the ABL top while being advected horizontally by the background flow. This implies a linear growth of the forest's internal boundary layer through the advected convective boundary layer. The growth of the ABL due to the change in surface properties follows the square-root law of a conventional slab model for an internal boundary layer, which should be applicable to other forests and to urban heat islands during convective conditions. In principle, our model can be used for the estimation of the growth of the ABL height for an increase of the surface roughness and heat flux over multiple step changes (e.g. the surrounding rural areas to the suburbs to the city centre), but this needs validation by measurements.

Appendix 1

Adjacent measurements for comparison of the ceilometer and Doppler lidar instruments were conducted during a preliminary campaign on 9 September 2013 at the forest site introduced in Sect. 2.2. The environmental conditions during these measurements were within the range of environmental conditions observed during the campaign in 2015 (Table 3). The ceilometer and Doppler lidar were of the same types used here, but a different instrument in case of the Doppler lidar. We compare the ABL height retrieval from the Doppler lidar and the ceilometer for the time period from 0800–1500 UTC for the comparison of the ABL height, because of

Table 3 Comparison of environmental conditions during the side-by-side measurement campaign on 9 September 2013 taken from Eder et al. (2015) (left column), and the campaign at the end of August 2015 (right column) at the forest site

u_* (m s^{-1})	0.72	0.57–0.73
$-z/L$	0.20	0.11–0.35
H (W m^{-1})	400.5	368.8–434.4
U (m s^{-1})	6.19	4.60–6.52

The rows show, from top to bottom, the mean values from 0500–1500 UTC of the friction velocity, stability parameter z/L, sensible heat flux and horizontal mean wind speed at 200–500 m above ground level. The value range for the 2015 campaign illustrates the minimum and maximum values
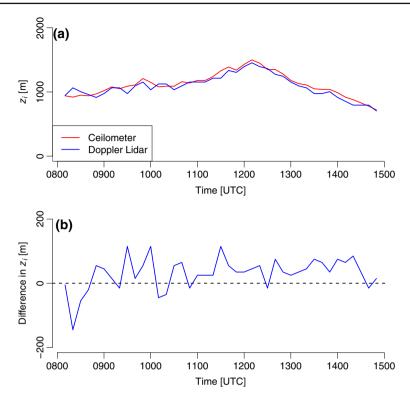
Fig. 7 Time series of ABL heights retrieved from side-by-side measurements of a ceilometer and a Doppler lidar (**a**) and the difference between the instruments (**b**)

the presence of clouds in the morning. The time series of the ABL height for both instruments are shown in Fig. 7; the time series of z_i values have a Pearson correlation coefficient of 0.96, a mean bias of 30.5 m, and a root-mean-square error of 48.3 m. The reasons for the bias may be different range-gate lengths, different laser wavelengths (which are sensitive to different aerosol sizes), or different window lengths for the vertical smoothing of the backscatter profiles (234 m for the Doppler lidar, and 240 m for the ceilometer).

References

Aubinet M, Vesala T, Papale D (2012) Eddy covariance: a practical guide to measurement and data analysis. Springer, Berlin, p 438

Baidya Roy S, Avissar R (2000) Scales of response of the convective boundary layer to land-surface heterogeneity. Geophys Res Lett 27(4):533–536

Baldocchi D, Falge E, Gu L, Olson R, Hollinger D, Running S, Anthoni P, Bernhofer C, Davis K, Evans R, Fuentes J, Goldstein A, Katul G, Law B, Lee X, Malhi Y, Meyers T, Munger W, Oechel W, Paw UKT, Pilegaard K, Schmid HP, Valentini R, Verma S, Vesala T, Wilson K, Wofsy S (2001) Fluxnet: a new tool to study the temporal and spatial variability of ecosystem-scale carbon dioxide, water vapor, and energy flux densities. Bull Am Meteorol Soc 82(11):2415–2434

Banerjee T, Katul G (2013) Logarithmic scaling in the longitudinal velocity variance explained by a spectral budget. Phys Fluids 25(12):125,106

Banerjee T, De Roo F, Mauder M (2017) Explaining the convector effect in canopy turbulence by means of large-eddy simulation. Hydrol Earth Syst Sci 21(6):2987

Barry RG, Chorley RJ (2003) Atmosphere, weather and climate, 8th edn. Routledge, New York, p 421

Batchvarova E, Gryning SE (1991) Applied model for the growth of the daytime mixed layer. Boundary-Layer Meteorol 56(3):261–274

Betts AK, Ridgway W (1989) Climatic equilibrium of the atmospheric convective boundary layer over a tropical ocean. J Atmos Sci 46(17):2621–2641

Browning KA, Wexler R (1968) The determination of kinematic properties of a wind field using doppler radar. J Appl Meteorol 7(1):105–113

Carson D (1973) The development of a dry inversion-capped convectively unstable boundary layer. Q J R Meteorol Soc 99(421):450–467

Dalu GA, Pielke RA, Baldi M, Zeng X (1996) Heat and momentum fluxes induced by thermal inhomogeneities with and without large-scale flow. J Atmos Sci 53(22):3286–3302

Dayan U, Rodnizki J (1999) The temporal behavior of the atmospheric boundary layer in israel. J Appl Meteorol 38(6):830–836

Dayan U, Lifshitz-Goldreich B, Pick K (2002) Spatial and structural variation of the atmospheric boundary layer during summer in Israel—profiler and rawinsonde measurements. J Appl Meteorol 41(4):447–457

De Tomasi F, Miglietta MM, Perrone MR (2011) The growth of the planetary boundary layer at a coastal site: a case study. Boundary-Layer Meteorol 139(3):521–541

De Wekker SFJ, Kossmann M (2015) Convective boundary layer heights over mountainous terrain—a review of concepts. Front Earth Sci 3:77

Deardorff JW (1970) Preliminary results from numerical integrations of the unstable planetary boundary layer. J Atmos Sci 27(8):1209–1211

Dupont S, Brunet Y (2008) Edge flow and canopy structure: a large-eddy simulation study. Boundary-Layer Meteorol 126(1):51–71

Eder F, Serafimovich A, Foken T (2013) Coherent structures at a forest edge: properties, coupling and impact of secondary circulations. Boundary-Layer Meteorol 148(2):285–308

Eder F, De Roo F, Rotenberg E, Yakir D, Schmid HP, Mauder M (2015) Secondary circulations at a solitary forest surrounded by semi-arid shrubland and their impact on eddy-covariance measurements. Agric For Meteorol 211:115–127

Foken T, Wichura B (1996) Tools for quality assessment of surface-based flux measurements. Agric For Meteorol 78(1):83–105

Garratt J (1990) The internal boundary layer: a review. Boundary-Layer Meteorol 50(1–4):171–203

Gopalakrishnan S, Avissar R (2000) An les study of the impacts of land surface heterogeneity on dispersion in the convective boundary layer. J Atmos Sci 57(2):352–371

Hennemuth B, Lammert A (2006) Determination of the atmospheric boundary layer height from radiosonde and lidar backscatter. Boundary-Layer Meteorol 120(1):181–200

Huang M, Gao Z, Miao S, Chen F, LeMone MA, Li J, Hu F, Wang L (2017) Estimate of boundary-layer depth over Beijing, China, using doppler lidar data during surf-2015. Boundary-Layer Meteorol 162(3):503–522

Juang JY, Porporato A, Stoy PC, Siqueira MS, Oishi AC, Detto M, Kim HS, Katul GG (2007) Hydrologic and atmospheric controls on initiation of convective precipitation events. Water Resour Res. https://doi.org/10.1029/2006WR004954

Kanani F, Träumner K, Ruck B, Raasch S (2014) What determines the differences found in forest edge flow between physical models and atmospheric measurements? An LES study. Meteorol Z 23(1):33–49

Kang SL, Lenschow D, Sullivan P (2012) Effects of mesoscale surface thermal heterogeneity on low-level horizontal wind speeds. Boundary-Layer Meteorol 143(3):409–432

Kröniger K, Banerjee T, De Roo F, Mauder M (2017) Flow adjustment inside homogeneous canopies after a leading edge—an analytical approach backed by les agricultural and forest meteorology. Agric For Meteorol 255:17–30

Lammert A, Bösenberg J (2006) Determination of the convective boundary-layer height with laser remote sensing. Boundary-Layer Meteorol 119(1):159–170

Lenschow D, Wyngaard JC, Pennell WT (1980) Mean-field and second-moment budgets in a baroclinic, convective boundary layer. J Atmos Sci 37(6):1313–1326

Lotteraner C, Piringer M (2016) Mixing-height time series from operational ceilometer aerosol-layer heights. Boundary-Layer Meteorol 161(2):265–287

Mahrt L (2000) Surface heterogeneity and vertical structure of the boundary layer. Boundary-Layer Meteorol 96(1):33–62

Maronga B, Raasch S (2013) Large-eddy simulations of surface heterogeneity effects on the convective boundary layer during the LITFASS-2003 experiment. Boundary-Layer Meteorol 146(1):17–44

Mauder M, Foken T (2015) Documentation and instruction manual of the Eddy-covariance software package TK3 (update). T Universität Bayreuth/Abteilung Mikrometeorologie, Bayreuth

Mauder M, Desjardins RL, MacPherson I (2007) Scale analysis of airborne flux measurements over heterogeneous terrain in a boreal ecosystem. J Geophys Res Atmos. https://doi.org/10.1029/2006JD008133

Mauder M, Cuntz M, Drüe C, Graf A, Rebmann C, Schmid HP, Schmidt M, Steinbrecher R (2013) A strategy for quality and uncertainty assessment of long-term eddy-covariance measurements. Agric For Meteorol 169:122–135

Moore C (1986) Frequency response corrections for eddy correlation systems. Boundary-Layer Meteorol 37(1–2):17–35

Münkel C, Eresmaa N, Räsänen J, Karppinen A (2007) Retrieval of mixing height and dust concentration with lidar ceilometer. Boundary-Layer Meteorol 124(1):117–128

Orlanski I (1975) A rational subdivision of scales for atmospheric processes. Bull Am Meteorol Soc 56:527–530

Päschke E, Leinweber R, Lehmann V (2015) An assessment of the performance of a 1.5 μm doppler lidar for operational vertical wind profiling based on a 1-year trial. Atmos Meas Tech 8(6):2251

Rotach MW, Wohlfahrt G, Hansel A, Reif M, Wagner J, Gohm A (2014) The world is not flat: implications for the global carbon balance. Bull Am Meteorol Soc 95(7):1021–1028

Rotenberg E, Yakir D (2010) Contribution of semi-arid forests to the climate system. Science 327(5964):451–454

Rotenberg E, Yakir D (2011) Distinct patterns of changes in surface energy budget associated with forestation in the semiarid region. Glob Change Biol 17(4):1536–1548

Schotanus P, Nieuwstadt F, De Bruin H (1983) Temperature measurement with a sonic anemometer and its application to heat and moisture fluxes. Boundary-Layer Meteorol 26(1):81–93

Seibert P, Beyrich F, Gryning SE, Joffre S, Rasmussen A, Tercier P (2000) Review and intercomparison of operational methods for the determination of the mixing height. Atmos Environ 34(7):1001–1027

Stull RB (1992) A theory for mixed-layer-top levelness over irregular topography. In: Proceedings of the 10th AMS symposium on turbulence and diffusion, Portland

Stull RB (1988) An introduction to boundary layer meteorology. Springer, Dordrecht

Sühring M, Maronga B, Herbort F, Raasch S (2014) On the effect of surface heat-flux heterogeneities on the mixed-layer-top entrainment. Boundary-Layer Meteorol 151(3):531–556

Sun J, Lenschow DH, Mahrt L, Nappo C (2013) The relationships among wind, horizontal pressure gradient, and turbulent momentum transport during CASES-99. J Atmos Sci 70(11):3397–3414

Tennekes H (1973) A model for the dynamics of the inversion above a convective boundary layer. J Atmos Sci 30(4):558–567

Träumner K, Kottmeier C, Corsmeier U, Wieser A (2011) Convective boundary-layer entrainment: short review and progress using doppler lidar. Boundary-Layer Meteorol 141(3):369–391

Träumner K, Wieser A, Ruck B, Frank C, Röhner L, Kottmeier C (2012) The suitability of doppler lidar for characterizing the wind field above forest edges. Forestry 85(3):399–412

Venkatram A (1977) A model of internal boundary-layer development. Boundary-Layer Meteorol 11(4):419–437

Wilczak JM, Oncley SP, Stage SA (2001) Sonic anemometer tilt correction algorithms. Boundary-Layer Meteorol 99(1):127–150

Wu Y, Nair US, Pielke RA, McNider RT, Christopher SA, Anantharaj VG (2009) Impact of land surface heterogeneity on mesoscale atmospheric dispersion. Boundary-Layer Meteorol 133(3):367–389

Zhong S, Doran JC (1995) A modeling study of the effects of inhomogeneous surface fluxes on boundary-layer properties. J Atmos Sci 52(17):3129–3142

Zilitinkevich SS, Tyuryakov SA, Troitskaya YI, Mareev EA (2012) Theoretical models of the height of the atmospheric boundary layer and turbulent entrainment at its upper boundary. Izv Atmos Ocean Phys 48(1):133–142